Parabolic microlensed optical fiber for coupling efficiency improvement in single mode fiber

Zaeid Bouhafs[1], Assia Guessoum[1], Abdelhak Guermat[1], Djamila Bouaziz[1,2,3], Sylvain Lecler[2,3], Nacer-Eddine Demagh[1]

[1]*Applied Optics Laboratory, Institute of Optics and Precision Mechanics, Ferhat Abbas University Setif1, Setif 19000, Algeria*
[2] *ICube, University of Strasbourg, UMR CNRS 7357 - ILLKIRCH 67412, France*
[3] *INSA de Strasbourg, Strasbourg, France*

*Corresponding author: ndemagh@univ-setif.dz, ndemagh@yahoo.fr

Abstract

The efficiency of optical coupling between an optical fiber and other components, be it a light source, a photodetector or another fiber, often depends on the performance of the focusing components. In optoelectronics, microlenses are generally incorporated at the end of optical fibers to ensure optimal coupling. These microlenses are primarily fabricated with a spherical profile easier to achieve, with a determined radius and low production costs. However, these microlenses exhibit a relatively large waist due to intrinsic spherical aberrations making difficult light coupling in single mode fiber. This article presents the study of a microlens with a parabolic profile made of polydimethylsiloxane (PDMS) at the end of a singlemode optical fiber (SMF 9/125). We investigate theoretically and experimentally the contribution of the parabolic profile compared to the spherical ones. Calculations at λ =1.31 µm show a decrease in the radius of the spot diagram in the focal plane divided by 3 from an RMS value of 623 nm in the spherical case, to 229 nm in the parabolic case. The measured optical coupling is improved by up to 100%. For the different studied microlens radii of curvatures, the value of the waists obtained varies from 1.00 µm to 4.90 µm with working distances from 5.80 to 48.80 µm respectively.

Keywords:

Parabolic microlens, micro-collimator, aspherical microlens, coupling efficiency, coupling optimization, spherical aberration.

1. Introduction

Effective coupling between laser diode sources (LD) and single mode fibers (SMF) or other optical components is an essential requirement in many applications, particularly in optical communication systems involving optical fiber connections. The propagation of light should then be properly collimated using appropriate microlenses. The latter are usually spherical with a simple geometric shape that can be described by a constant radius of curvature. Various studies have been conducted on micro-collimators embedding spherical and hemispherical microlenses [1, 2, 3, 4]. Although these microlenses are simple to manufacture and inexpensive, their performance is, however, affected by induced spherical aberrations. This defect, inherent to their geometry, is at the origin of the widening of the focusing spot. To avoid these aberrations, aspherical structures with non-constant bending radii are employed; the complex shape of the microlenses allows for the correction of spherical aberrations. In this case, the profiles are more complex and can be described analytically by a radius of curvature composed of several terms of higher order coefficients. The approximation to the first terms of the development shows, as for classical lens, that the parabolic microlens is a prime candidate

for the addition of such microlenses to optical fibers. This results in a narrower focusing spot, ensuring thereby better coupling efficiency.

To correct aberrations and optimize light transfer, various aspherical microlenses were investigated, essentially elliptical, conical, hyperbolic and parabolic. S. H. Ghasemi et al. [5] presented a study on aspherical plano-convex aspherical lenses and showed that they correct aberrations that would be produced by an equivalent conventional lens. Jhy-Cherng Tsai et al. [6] proposed to reduce aberrations by forming a biconvex structure by juxtaposing two microlenses. In this case, the aberrations are reduced but not as much as in aspherical shapes. Yu-Kuan Lu et al. [7] obtained a high coupling rate using elliptical microlenses. These structures are more suitable when it comes to coupling light from an axially non-symmetrical source to optical fibers. They compensate for the asymmetry of the beam but they are not intended for correcting aberrations. Rahman et al. [8] investigated optical coupling between an LD source and a truncated conical microlens micro-collimator. By this process, they obtained an increase in the coupling rate by taking into account only the multiple reflections between the two surfaces of the components. S. D. Alaluri. [9] presented a comparative study on the coupling efficiency between two SMF (Fiber coupling efficiency) fibers using spherical, conical and GRIN rod lens microlenses. Under optimal conditions, a coupling > 91% was recorded for the spherical microlens. It is lower compared to the other microlenses; however, it offers the advantage of being the least sensitive to angular misalignment (Tilt), and allows therefore for satisfactory tolerances during component alignment. Aberrations remain the main causes of the weakening of the coupling. Gangopadhyay [10] and C-H. Tien [11] used microlenses with hyperbolic profiles to prevent the effects of aberrations. The widths of the focusing spots found were smaller than those obtained using spherical lenses with the same characteristics. A. K. Das et al. [12] introduced a microlens design of a planar type (step index planar microlens) based on multilayer deposition of doped polymer, of variable refractive index, on a concave surface. They were able to reduce spherical aberrations by correcting the path of light. M. Thual et al. [13-14] demonstrated the possibility to obtain narrow focusing properties by combining a GRIN with a glass hemispherical microlens and more recently, sub-wavelength photonic nanojet focusings were obtained by Lecler [15], but requires large mode area fiber.

All studies generally aim to improve the coupling; as such, the introduction of calculation based on the ABCD matrix transformation method simplifies the calculation of coupling efficiency. This calculation was widely adopted for optical fibers incorporating microlenses of different profiles and, in particular, in the parabolic profile [16] where it was shown that the coupling efficiency can reach 100% under optimal conditions (not taking into account internal reflection).

In this work, a study is presented on the characteristics and performance of an SMF optical fiber (9/125µm) microlens manufactured with a parabolic profile. The optical propagation through the microlens is computed using the ABCD transformation matrix method, which allows for the determination of its main characteristics such as focus waist and working distance. It is shown that this parabolic microlens offers better coupling performance compared to microlenses with an equivalent hemispherical shape.

2. Characterization and analysis of aberration

We consider in our study the optical system in Fig. 1, composed of an SMF fiber with a parabolic microlens of refractive index n_s and radius of curvature R at the apex. It is therefore necessary to study the propagation through the microlens and determine the important parameters of the transmitted beam, including the waist (w_l) and the working distance (Z).

The beam propagation through this microlens follows the path indicated in Fig. 1. The wave guided by the SMF mode width fiber SMF ($2w_0$) is projected by the microlens into a waist image (w_l).

The mode width $2w_0$ is calculated using the following Marcuse formula [17],

$$\frac{w_0}{a} = 0.65 + \frac{1.619}{V^{3/2}} + \frac{2.879}{V^6} \quad (1)$$

where a is the radius of the core of the single mode fiber which is 4.5 µm for a 9/125 µm fiber and V is the normalized frequency given by the expression below:

$$V = \frac{2\pi}{\lambda} a\sqrt{n_1^2 - n_2^2} \quad (2)$$

with n_1 and n_2 the core and cladding indices respectively, and λ is the free space wavelength used, λ =1.31 µm. Calculations give $w_0 = 4.1$ µm.

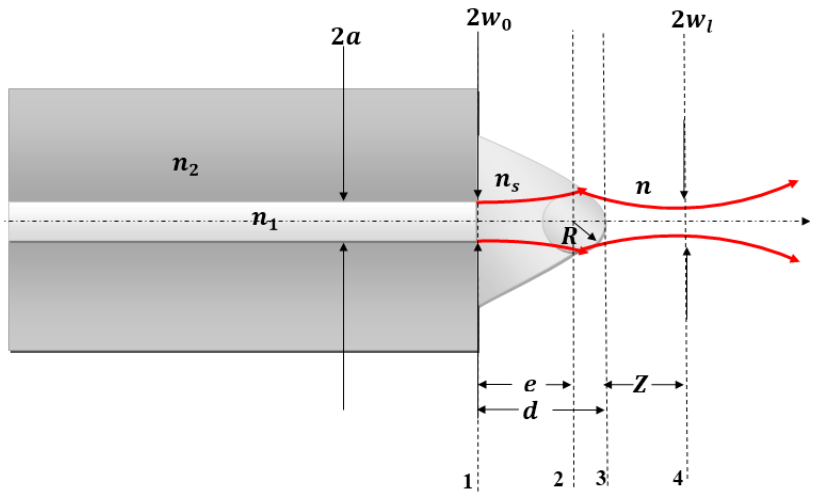

Fig.1. Light propagation through the microlens.

Calculation of the mode field width $2w_0$ allows for the determination of other optical characteristics, including the new waist (w_l) and the working distance (Z), using the transfer matrix M of the optical system. This matrix can be broken down into 3 elementary matrices corresponding to the different propagation media. It is written as follows:

$$M = M_{34}M_{23}M_{12} \quad (3)$$

Where $\mathrm{M}_{12}, \mathrm{M}_{23}$ et $\mathrm{M}_{3,4}$ are elementary matrices corresponding, respectively, to the transfer matrix of the propagation medium between planes 1 and 2, the transfer matrix of the parabolic microlens between planes 2 and 3, and that of the image waist formation medium between planes 3 and 4 in air with index n_0.

Considering the ABCD law, we obtain the following equation [18]:

$$\mathrm{M} = \begin{pmatrix} A & B \\ C & D \end{pmatrix} = \begin{pmatrix} 1 & Z \\ 0 & 1 \end{pmatrix} \begin{pmatrix} 1 & 0 \\ \frac{n_0 - n_s}{n_0\, p} & \frac{n_s}{n_0} \end{pmatrix} \begin{pmatrix} 1 & \frac{d}{n_s} \\ 0 & 1 \end{pmatrix} \tag{4}$$

with

$$\mathrm{M}_{12} = \begin{pmatrix} 1 & \frac{d}{n_s} \\ 0 & 1 \end{pmatrix} \tag{5}$$

$$\mathrm{M}_{23} = \begin{pmatrix} 1 & 0 \\ \frac{n_0 - n_s}{n_0\, p} & \frac{n_s}{n_0} \end{pmatrix} \tag{6}$$

$$\mathrm{M}_{34} = \begin{pmatrix} 1 & Z \\ 0 & 1 \end{pmatrix} \tag{7}$$

where d is the thickness of the microlens and p is the focal parameter of the parabolic profile. The apex can be described by an inscribed circle of radius $R = p$ [19],

From Eq. (4), we can deduce the parameters A, B, C et D as follows:

$$A = 1 + Z\left(\frac{n_0 - n_s}{n_0\, R}\right) \tag{8}$$

$$B = \frac{d}{n_s} + \frac{d}{n_s} Z \left(\frac{n_0 - n_s}{n_0\, R}\right) + Z\frac{n_s}{n_0} \tag{9}$$

$$C = \frac{n_0 - n_s}{n_0\, R} \tag{10}$$

$$D = \frac{d}{n_s}\frac{n_0 - n_s}{n_0\, R} + \frac{n_s}{n_0} \tag{11}$$

The new waist w_l and the working distance Z [20] are deduced from Eq. (12) and (13) as follows:

$$AC + g^2 BD = 0 \tag{12}$$

$$w_l = w_0 \left(\frac{n_s}{n_0}\, \frac{A^2 + g^2 B^2}{AD - BC}\right)^{1/2} \tag{13}$$

where

$$g = \frac{\lambda}{\pi w_0^2 n_s} \tag{14}$$

By solving the previous equations, we deduce the working distance Z and the waist w_l which take the following forms:

$$Z = -\frac{1+g^2 d\left(\frac{d}{{n_s}^2}+\frac{R}{1-n_s}\right)}{\frac{1-n_s}{R}+g^2 d\left(\frac{d}{{n_s}^2}\frac{1-n_s}{R}+2+\frac{{n_s}^2}{d}\frac{R}{1-n_s}\right)} \quad (15)$$

$$w_l = w_0\left(1+\frac{g^2 d^2}{{n_s}^2}+\frac{g^2 dZ(1-n_s)}{R}\left[\frac{2}{g^2 d}+\frac{2d}{{n_s}^2}+\frac{2R}{1-n_s}+Z\left(\frac{1-n_s}{g^2 dR}+2+\frac{d(1-n_s)}{{n_s}^2 R}+\frac{{n_s}^2 R}{d(1-n_s)}\right)\right]\right)^{1/2} \quad (16)$$

2.1. Characterization of the microlens profile

Fig. 2 shows a magnified view of a typical polydimethylsiloxane (PDMS) parabolic microlens attached to the end of an SMF optical fiber (9/125 µm). The profile of the microlens is determined by image processing. Indeed, starting from the experimental image in Fig. 2, the coordinates of the points of the microlens contour are extracted and represented by the points as shown in Fig. 3.

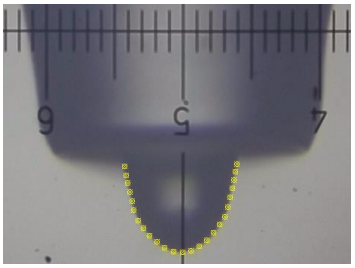

Fig.2. Profile of the parabolic microlens at the end of a fiber (SMF 9/125). High (thickness) of 50 µm, base width of 54 µm and bending radius R = 17.5 µm. (•••) Extraction of the contour points of the parabolic microlens.

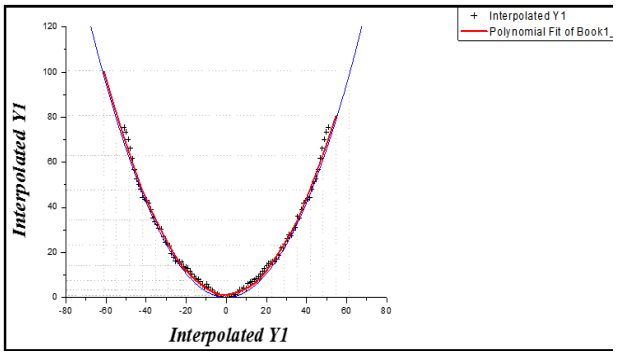

Fig.3. Representation of the experimental points of the microlens contour and the continuous line interpolation function.

These points are then interpolated by a function of the form $y=a.x^b$ to determine its profile. The parameters (a and b) are determined by power regression. The calculations give the following values:

$a = 0.0277$

$b = 2.1153$

with a residue of 1.0×10^{-13}

Then, the profile equation is written as follows:

$$y = 0.0277\ x^{2.1} \quad (17)$$

Figure 3 shows the experimental points and the parabolic interpolation curve.

2.2. Correction of spherical aberrations by a parabolic microlens

A spherical aberration is an aperture defect due to the spherical shape of the lens. The light rays coming from a point at infinity are deflected differently according to their distance from the optical axis. The

rays furthest from the optical axis converge more than the paraxial rays, which leads to the appearance of different image foci on the optical axis.

The spherical aberration thus appears in two dimensions: along the optical axis with different image focal points, and around the optical axis with diffusion spots of different diameters. This is why two types of spherical aberrations can be distinguished. The longitudinal spherical aberration equivalent to the distance between the marginal focus and the paraxial focus, and the transverse spherical aberration, which measures the radius of the diffusion spot at the paraxial focus. One of the usual strategies to correct these aberrations is the use of a parabolic profile. Indeed, the latter has proven to be effective in minimizing these aberrations [21].

The aspherical surface schematized in Figure 4 can be represented by parameters based on geometric equations, namely a radius of curvature R at the apex and a transverse radius r varying radially from the center to the edge.

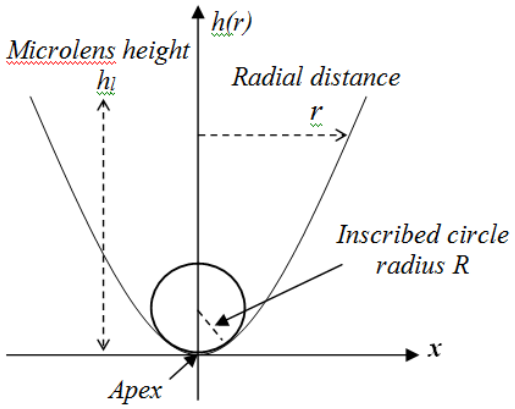

Fig.4. Diagram of an aspherical surface

This profile is described by the function $h(r)$, which represents the height of the aspherical microlens as a function of the radial distance r to the optical axis. It is expressed as follows [22]:

$$h(r) = \frac{1}{R}\frac{r^2}{1+\sqrt{1-(1+K)\frac{r^2}{R^2}}} + A_4\, r^4 + A_6\, r^6 + A_8\, r^8 + \cdots \qquad (18)$$

where A_i are constants calculated and given according to the geometric profile and parameters of the desired microlenses.
K is the aspheric constant [23]. The lens profile h(r) is considered as spherical if (K = 0), elliptic if (-1<K<0 or k>0), hyperbolic if (K < -1) and parabolic if (K = -1). The last case concerns this research work.

The radius of curvature at the vertex is given by the expression

$$R = (K+1)\frac{h_l}{2} + \frac{r^2}{2h_l} \qquad (19)$$

where h_l is the height of the microlens.

The back focal length of a plano-convex refractive lens is given by:

$$f = \frac{R}{n-1} = \frac{1}{2(n-1)}\left((K+1) + \frac{r^2}{h_l}\right) \quad (20)$$

where n is the refractive index of the microlens.

The spherical aberration coefficient of a microlens is given by [24]:

$$S = (ON)^4 f \frac{n^2}{(n-1)^2} \quad (21)$$

where $ON = \frac{r}{f}$ represents the numerical aperture.

Then, the spherical aberration coefficients of a spherical microlens S_{sph} and a parabolic microlens S_{par} are written respectively as follows:

$$S_{sph} = (ON)^4 \left(\frac{h_l}{2} + \frac{r^2}{2h_l}\right) \frac{n^2}{(n-1)^3} \quad (22)$$

$$S_{par} = (ON)^4 \left(\frac{r^2}{2h_l}\right) \frac{n^2}{(n-1)^3} \quad (23)$$

The difference in the correction of spherical aberrations between these two microlenses is estimated by the following expression:

$$\mathrm{D} = \left(1 - \frac{S_{par}}{S_{sph}}\right) \quad (24)$$

The calculation of the aberration coefficient S_{par} (Eq. 23) of the studied parabolic microlenses and that of the coefficient S_{sph} of the spherical microlenses (Eq. 22) with the same radius of curvature are reported in Table 1 and the corresponding variation curves are shown in Figures 5(a) and 5(b). The aberrations are clearly lower for parabolic microlenses.

The minimum of aberration $S_{par} = 0.229$ µm is achieved for an optimal curvature radius R = 9.5 µm, and as a result, an improvement of D by ~ 63% is achieved.

Tab.1. Comparison of the aberration values of the parabolic microlenses and the spherical microlenses with the same radius of curvature and refractive index.

R(µm)	$S_{par}(\mu m)$	$S_{sph}(\mu m)$	Improvement D (%)
2.50	0.426	0.800	46
9.50	0.229	0.623	63
13.50	0.328	0.736	55
17.50	0.552	0.988	44
21.00	0.920	1.478	38

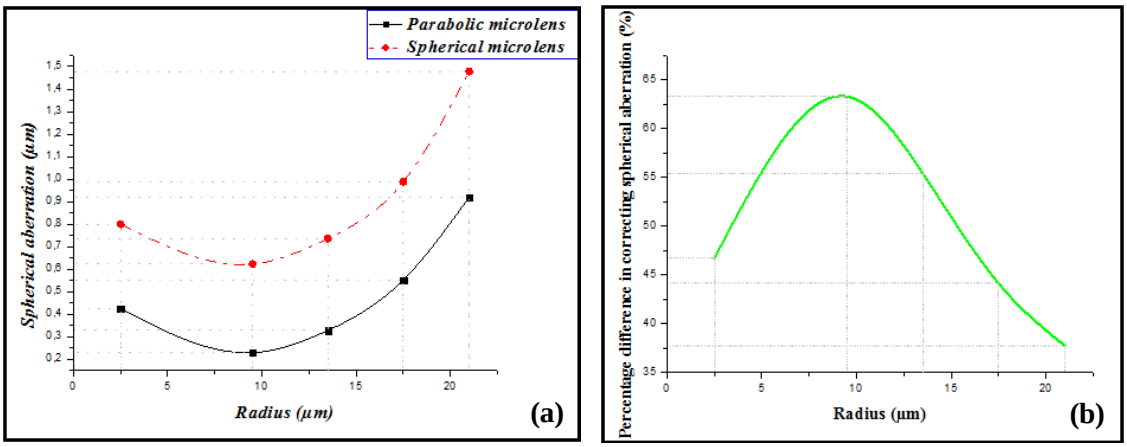

Fig. 5. (a) Spherical aberrations as a function of the radii of curvature of spherical and parabolic microlenses. **(b)** Improvement D with parabolic microlenses compared to equivalent spherical microlenses.

The spherical aberrations cause a broadening of the spot diagram. To illustrate it, the spot diagrams obtained by OSLO simulations are shown in Fig. 6(a) and 6(b). This results in an RMS geometric radius of the spot diagram of 0.229 µm for the parabolic case, around 3 times smaller than that of the spherical case with an RMS radius of 0.623 µm,.

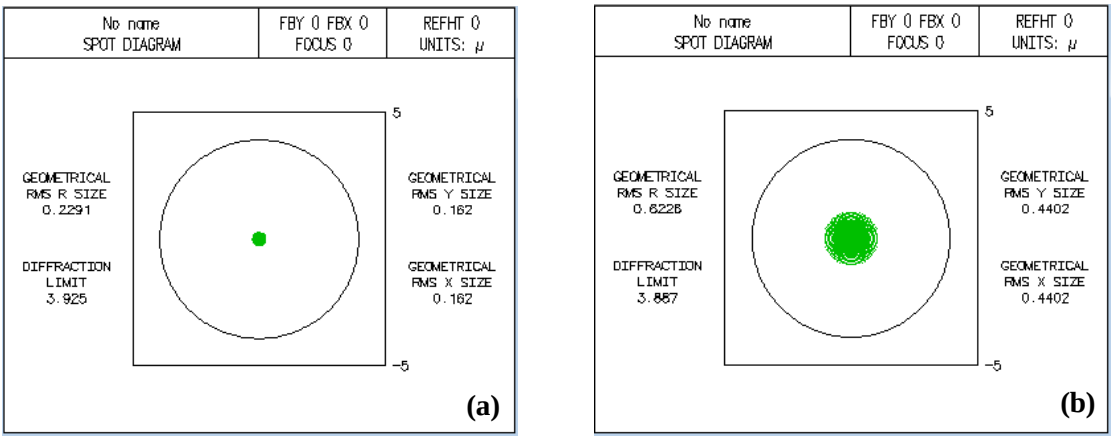

Fig. 6. Representation of the spherical aberration spot. In **(a)** the case of the parabolic microlens of R = 9.50 µm and **(b)** the case of the spherical microlens of the same R = 9.50 µm.

3. Calculation of the coupling efficiency and optimization of the bending radius of the microlenses

The coupling efficiency between a source and a fiber, via a parabolic microlens, placed at the end of the fiber is given [25] by the following integral:

$$\eta = \frac{\left|\iint \psi_r \psi_f^* \mathrm{dxdy}\right|^2}{\iint \left|\psi_r\right|^2 \mathrm{dxdy} \iint \left|\psi_f\right|^2 \mathrm{dxdy}} \qquad (25)$$

where ψ_r and ψ_f represent, respectively the field of the beam transformed by a microlens and the mode field of the cleaved SMF optical fiber.

Fig. 7 shows the coupling between two Gaussian beams, one with a waist w_l and a wave curvature radius R_l emanating from a 9/125 SMF fiber with a microlens; the other is the $2w_f$ mode diameter of a cleaved 4/125 SMF fiber. R_f is its wave curvature radius. The distance between the two waists is L.

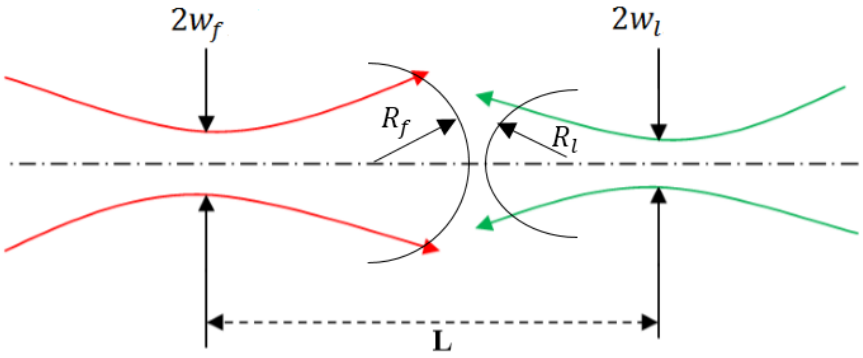

Fig. 7. Coupling between two Gaussian beams. Light propagates from left to right.

In this case, the coupling efficiency η is expressed in a simple form [26], given by the expression:

$$\eta = \frac{2w_f w_l}{\sqrt{\left(w_f^2+w_l^2\right)^2 + \frac{\lambda^2 L^2}{\pi^2}}} \tag{26}$$

To calculate the coefficient η, we will determine w_f and w_l. The radius (waist) of the mode of the 4/125 µm cleaved fiber is calculated from the Marcuse equation: $w_f = 2.28$ µm. w_l of the microlens is experimentally determined in what follows.

4. Experimental set-up for characterizing the microlens

4.1. Determination of the waist and of the working distance

The experimental characterization consists of determining the optical parameters, namely the waist of the microlenses, the working distance, the optimal bending radius and the efficiency of the optical coupling. For this purpose, the experimental set-up dedicated to the characterization is shown in Fig. 8.

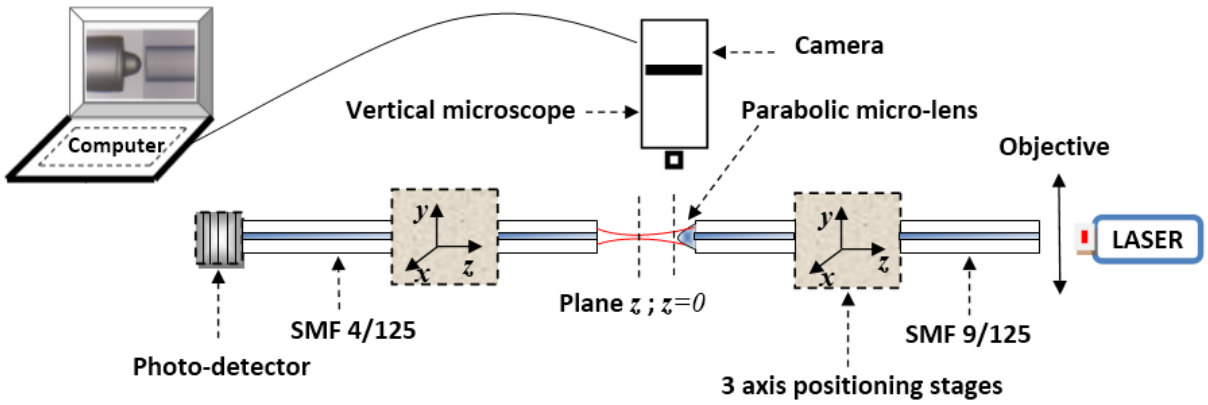

Fig. 8. Experimental set-up for the characterization of microlenses with parabolic microlenses.

The set-up is composed first by a laser source (λ = 1,31µm) coupled into a 9/125 fiber with a microlens by a microscope lens (x10). Then, an acquisition system composed of a CCD camera combined with a vertical microscope is used to control the centering and alignment of the parabolic microlens tip in front of a 4/125 µm "measurement" fiber going to a photo-detector. The latter is used to scan the output beam in both perpendicular directions (***x*** and ***y***) of the transverse plane on the one hand, and in the axial direction ***z*** on the other hand. The microlens and the measuring fiber are fixed on 3D micro-displacement systems. The nanometric displacement in the ***z*** direction is ensured by a piezo-positioner (Edmund PP-30). The longitudinal and transverse translation of the measurement fiber allows to scan, the beam profile of the coupling area from the surface of the microlens (***z*** = 0). The photodetector gives the value of the coupled light intensity.
At the maximum of the optical coupling, the working distance Z and the image waist w_l are deducted. For this purpose, five different microlenses were characterized following the same procedure.

4.2 Results and discussions

Measurements of the transmitted light intensity were taken in a scanned coupling volume of 12 µm in the transverse plane and 40 µm in the axial direction in 1 µm steps with a resolution of 10 nm. The experimental values were then interpolated by a Gaussian distribution as shown in Fig. 9(a). These variation curves show the scanned coupling volume.

From the longitudinal section of the curves (Fig. 9(b)), the working distance Z, starting from the surface of the microlens (***z*** = 0) to the maximum of the curve, is deduced. From the transverse curve at the minimum width of the coupling volume, in this case at Z = 21, the waist of the focus spot is determined.

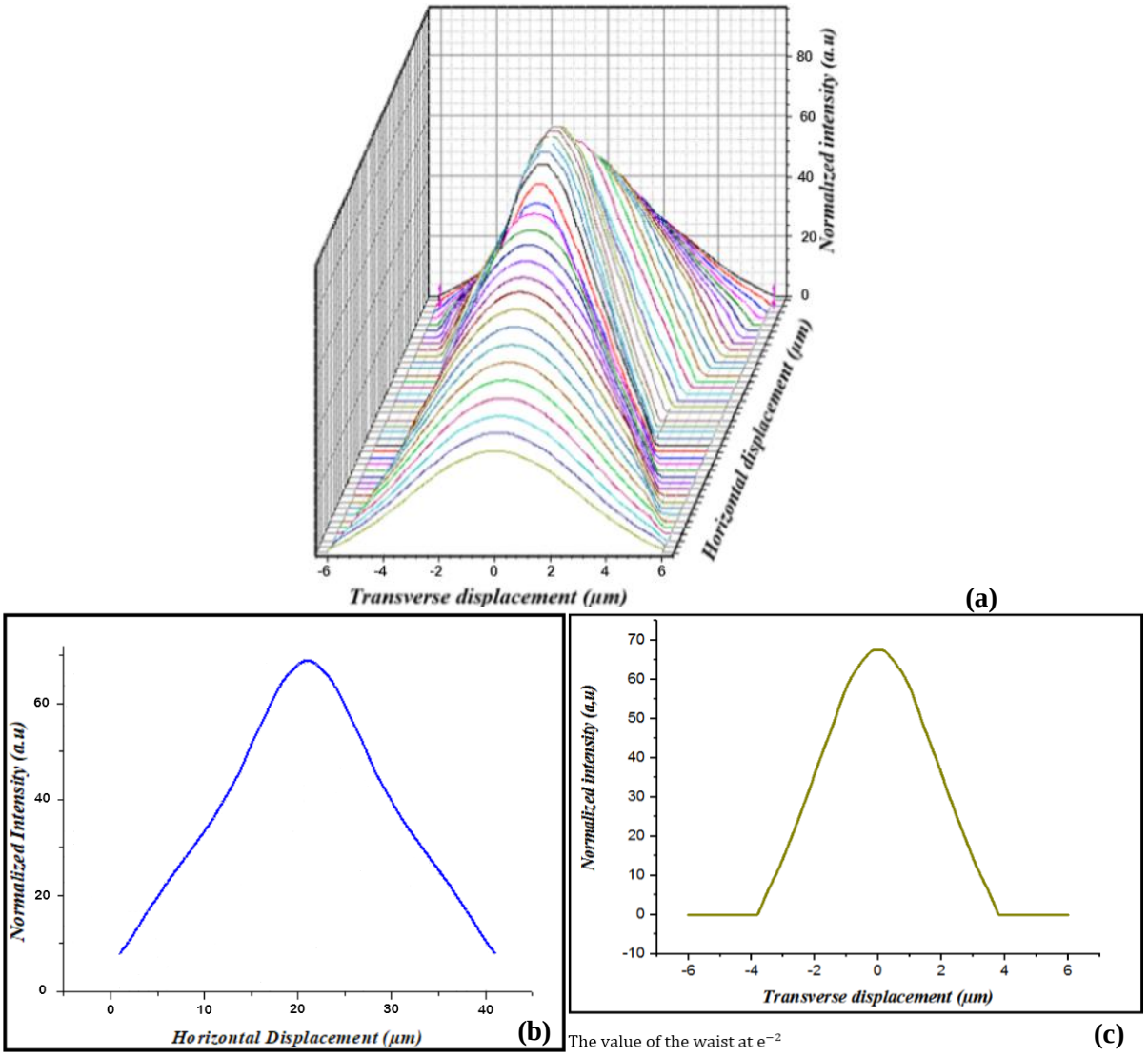

Fig. 9. Coupling between a 9/125 fiber (with microlens) and a 4/125 fiber. **(a)** Representation of the Gaussian interpolation curves (41) of the experimental values in the coupling volume from z = 21 µm (front curve) to z = 41 µm (back curve). **(b)** Longitudinal section of the coupling volume. **(c)** Transversal section at the minimum width of the coupling volume.

In Fig. 9, the measurements concern a single case of microlens. Therefore, in order to optimize the coupling, it is essential to find the optimal microlens bending radius yielding the best performance. Figures 10 (a) and (b) show, respectively, the theoretical and experimental curves of the variation of the waist and the working distance as a function of the radius of curvature of the parabolic microlenses in PDMS with index $n_s = 1.418$, integrated on a 9/125 µm single mode fiber at λ = 1.31µm.

The curves are monotonous within the range of the studied radii of curvature (2.5 µm – 21 µm). The optimal bending radius corresponds to the maximum coupling value. For this purpose, the variation of the coupling coefficient η (Eq. 26) as a function of the bending radius of the microlenses is shown in Fig. 10(c). The curve passes through a maximum of 100% for R = 10.08

µm (Internal reflections are not taken into account). The approximate experimental value corresponds to the radius of curvature $R_{opt} = 9.50$ µm, yielding a coupling $\eta_{exp} \sim 99\%$.

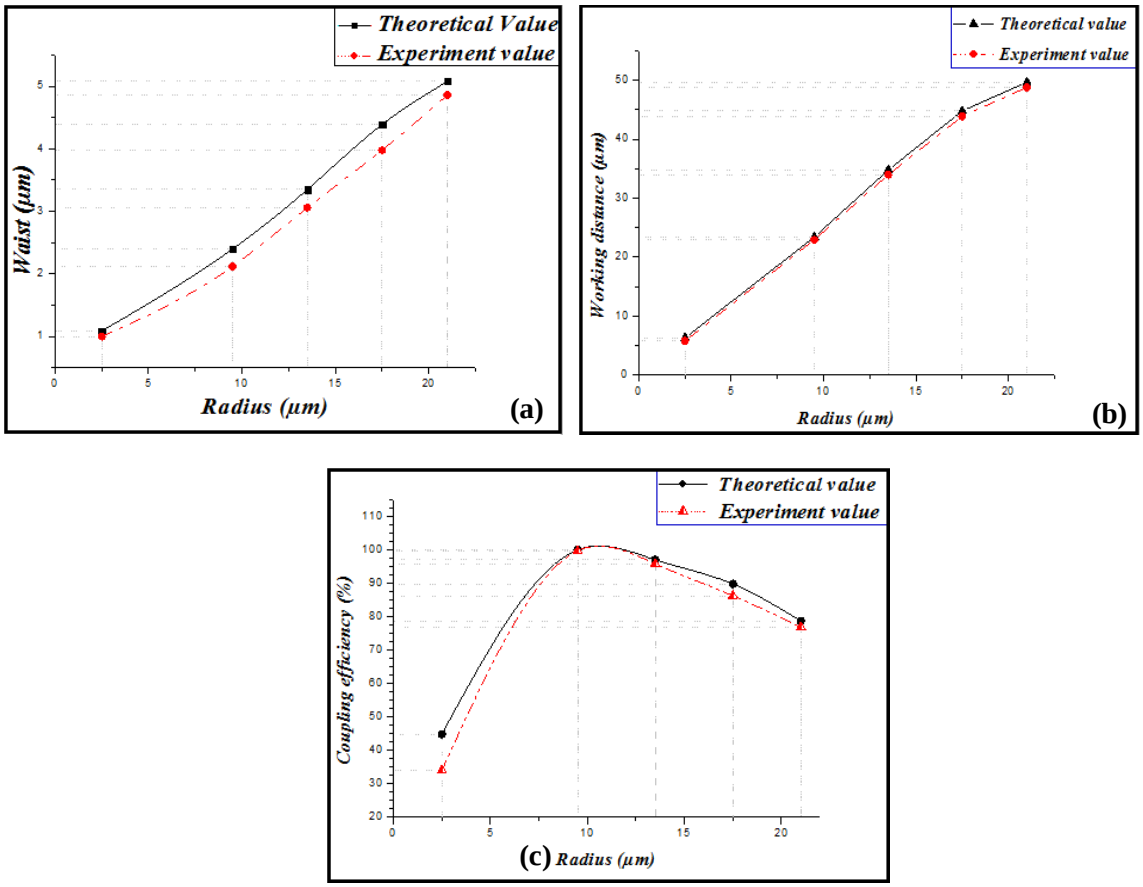

Fig. 10. Theoretical and experimental curves corresponding to **(a)** the waist, **(b)** the working distance, **(c)** the coupling efficiency, as a function of the curvature radius of the microlenses.

Table 2 summarizes the results.

Tab.2. Characteristics of the five different microlenses studied. With $w_f = 2.28$ µm and $\lambda = 1.31$ µm

R(µm)	$Z_{theo}(\mu m)$	$Z_{exp}(\mu m)$	$w_{l\,theo}(\mu m)$	$w_{l\,exp}(\mu m)$	$\eta_{theo}(\%)$	$\eta_{exp}(\%)$
2.50	***6.32***	**5.80**	**1.09**	**1.00**	**44.85**	**34.04**
09.50	***23.41***	**22.95**	**2.30**	**2.12**	**<100**	**99.73**
13.50	***34.80***	**34.00**	**3.35**	**3.06**	**97.02**	**95.82**
17.50	***44.80***	**43.90**	**4.39**	**3.98**	**89.80**	**86.26**
21.00	***49.68***	**48.80**	**5.08**	**4.86**	**78.71**	**76.90**

The value of the waists obtained experimentally varies from 1.00 µm to 4.90 µm with working distances from 5.80 to 48.80 µm respectively. We can deduce that the most suitable fabricated microlens corresponds to a radius of curvature $R_{opt} = 9.50\ \mu m$. Theoretically, the maximum coupling of the curve corresponds to R = 10.08 µm

5. Conclusion

The objective of this work was focused on optimizing optical coupling where aberrations induced by spherical microlenses are considered. To this end, the theoretical and experimental performances of microlenses with parabolic microlenses have been studied. The profile of these microlenses was determined using image processing by extracting their contours. The interpolation of the points allowed the determination of the radius of curvature at the apex and the calculation of the aberration coefficient. The results show that there is a 63% reduction in aberrations with the parabolic microlenses compared to the spherical one, resulting in a reduction of the spot size. Hence, optical coupling with any other passive or active component can be improved. In this regard, the coupling efficiency was also optimized with respect to the bending radius of the microlenses. Among the five microlenses studied, the experimental value found a maximum coupling for R_{opt} = 9.50 µm near the maximum theoretical value R = 10.08 µm. In addition, the microlenses were characterized on a dedicated experimental bench where the coupling zone was analyzed in a volume axially greater than the Rayleigh distance. At the maximum coupling, the main optical parameters are determined, in particular the waist, the working distance and the coupling rate. As can be seen from the results, the performance obtained is in favor of the use of parabolic microlenses. These optical components can find suitable applications in optical connections and near-field surface analysis.

References

[1] J. Kim, M. Han, S. Chang, Jhang W. Lee, and K. Oh, Achievement of Large Spot Size and Long Collimation Length Using UV Curable Self-Assembled Polymer Lens on a Beam Expanding Core-Less Silica Fiber, IEEE photonics technology letters, 16(11), 2004. Doi : 10.1109/LPT.2004.834907

[2] X. Zhou, Z. Chen, Z. Wang, and J.Hou, Monolithic fiber end cap collimator for high-power free-space fiber–fiber coupling, Applied Optics, 55(15), 2016. http://dx.doi.org/10.1364/AO.55.004001.

[3] M. Zaboub, A. Guessoum, N.E. Demagh, A. Guermat, Fabrication of polymer microlenses on single mode optical fibers for light coupling,Optics Communications 366, p.122–126, 2016. http://dx.doi.org/10.1016/j.optcom.2015.12.010.

[4] K. Shiraishi, A new lensed fiber configuration employing cascaded Gi-fiber chips, J. Lightwave Technol. 18, p.787–794, 2000. Doi: S 0733-8724(00)05082-9.

[5] S.H. Ghasemi, M. R. Hantehzadeh, J. Sabbaghzadeh, D. Dorranian, V.Vatani, A. Babazadeh, K. Hejaz, A. Hemmati, M. Lafouti, Designing plano-convex aspheric lens for fiber optics collimator, Optics and Lasers in Engineering, 50 p.293–296, 2012.

Doi:10.1016/j.optlaseng.2011.07.014.
[6] J.C.Tsai, M. F. Chen, and H. Yang, Design and Fabrication of High Numerical Aperture and Low Aberration Bi-Convex Micro Lens Array, DTIP, 9-11(4), 2008. 978-2-35500-006-5. Doi : 978-2-35500-006-5.
[7] Hu, J.-Y., Lin, C.-P., Hung, S.-Y., Yang, H., & Chao, C.-K. (2008). Semi-ellipsoid microlens simulation and fabrication for enhancing optical fiber coupling efficiency. Sensors and Actuators A: Physical, 147(1), p.93–98, 2008. Doi:10.1016/j.sna.2008.04.005.
[8] F. A. Rahman, K. Takahashi, C. H. Teik, Theoretical analysis of coupling between laser diodes and conically lensed single-mode fibers utilizing *ABCD* matrix method, Opt. Commun. 215, p.61–68, 2003. Doi : S00 3 0-4 0 18 (0 2)0 21 9 3- 4.
[9] S. D. Alaruri, Single-mode fiber-to-single-mode fiber coupling efficiency and tolerance analysis: comparative study for ball, conic and GRIN rod lens coupling schemes using Zemax Huygen's integration and physical optics calculations. Optik - International Journal for Light and Electron Optics, 126(24), p.5923–5927, 2015. Doi:10.1016/j.ijleo.2015.09.176
[10] S. Gangopadhyay, S. Sarkar, *ABCD* matrix for reflection and refraction of Gaussian light beams at surfaces of hyperboloid of revolution and efficiency computation for laser diode to single-mode fiber coupling by way of a hyperbolic lens on the fiber tip, Appl. Opt. 36, p.8582–8586, 1997. Doi: S0030-4018(96)00328-8.
[11] C. H. Tien, Y. C. Lai, T. D. Milster and H.P.D.Shieh, Design and Fabrication of Fiber lenses for Optical Recording Applications, Jpn. J. Appl. Phys. 41, p. 1834–1837, 2002. Doi : 10.1143/JJAP.41.1834.
[12] A.K. Das, A.K. Ganguly. & all, Multi - layered step index micro - lens of low spherical aberration, SPIE Vol. 3557, 0277-786X (1998). Doi:http://proceedings.spiedigitallibrary.org/ on 01/20/2016.
[13] M. Thual, G. Moreau, J. Ribette, P. Rochard, M. Gadonna, et J.C. Simon, Micro-Lens on Polarization Maintaining Fibre for Coupling with 1.55µm Quantum Dot Devices, Optics Communications 255(4-6) p. 278-85, 2005. Doi.org/10.1016/j.optcom.2005.06.040
[14] Si Dat Le, et al. Study of Optimized Coupling Based on Micro-Lensed Fibers for Fibers and Photonic Integrated Circuits in the Framework of Telecommunications and Sensing Applications, Communications in Physics 26(4), p. 325, 2017.
https://doi.org/10.15625/0868-3166/26/4/8951
[15] R. Pierron, G. Chabrol, S. Roques, P. Pfeiffer, J-P. Yehouessi, G. Bouwmans and S. Lecler, Large-Mode-Area Optical Fiber for Photonic Nanojet Generation, Optics Letters 44(10): 2474, 2019. Doi.org/10.1364/OL.44.002474
[16] H. Z. Liu, The approximate matrix for a parabolic lens of revolution and its application in calculating the coupling efficiency, Optik 119, p.666–670, 2008.
Doi:10.1016/j.ijleo.2007.01.014
[17] D. Marcuse, Loss analysis of single-mode fiber splices. Bell Syst. Tech. J. 56, p.703–718, 1977. Doi:10.1002/j.1538-7305.1977.tb00534.x
[18] S. Mukhopadhyay, Coupling of a laser diode to single mode circular core graded index fiber via parabolic microlens on the fiber tip and identification of the suitable refractive index profile with consideration for possible misalignments, Journal of Optics, 45(4), p.312–323, 2016. Doi:10.1007/s12596-016-0311-z
[19] M. Do Carmo, Differential geometry of curves and surfaces, Prentice Hall, 1976.

[20] W. Emkey, C. Jack, Analysis and evaluation of graded-index fiber lenses. Journal of Lightwave Technology, 5(9) p.1156–1164, 1987. Doi:10.1109/jlt.1987.1075651
[21] S. Vazquez-Montiel and O. Garcıa-Lievanos, Spherical aberration correction using aspheric surfaces with an analytic-numerical method, Revista Mexicana de Fisica 59, p.273–281, 2013. Doi : PACS: 42.15-I; 42.15.Dp; 42.15.Eq; 42.15.Fr
[22] D, Mcister, Aspheric lenses: optics and applications Lens Talk, 26(25), 1998.
[23] Ph. Nussbaum, R. Volkely, H. P. Herzig, M. Eisner and S. Haselbeck, Design, fabrication and testing of microlens arrays for sensors and microsystems, Appl. Opt. 6, p.617–636, 1997. Doi: S0963-9659(97)86784-0
[24] H. P. Herzig (ed) 1997 Micro-optics (London: Taylor and Francis)
[25] S. N. Sarkar, B. P. Pal, K. Thyagarajan, Lens Coupling of Laser Diodes to Monomode Elliptic Core Fibers. Journal of Optical Communications, 7(3), p.92–96, 1986. Doi:10.1515/joc.1986.7.3.92.
[26] W.B. Joyce, B.C. DeLoach, Alignment of Gaussian beams, Appl. Opt. 23 (23), p.4187–4196, 1984.